

# Historical land use and land cover change reduced the temperature of cold extremes more than that of hot extremes

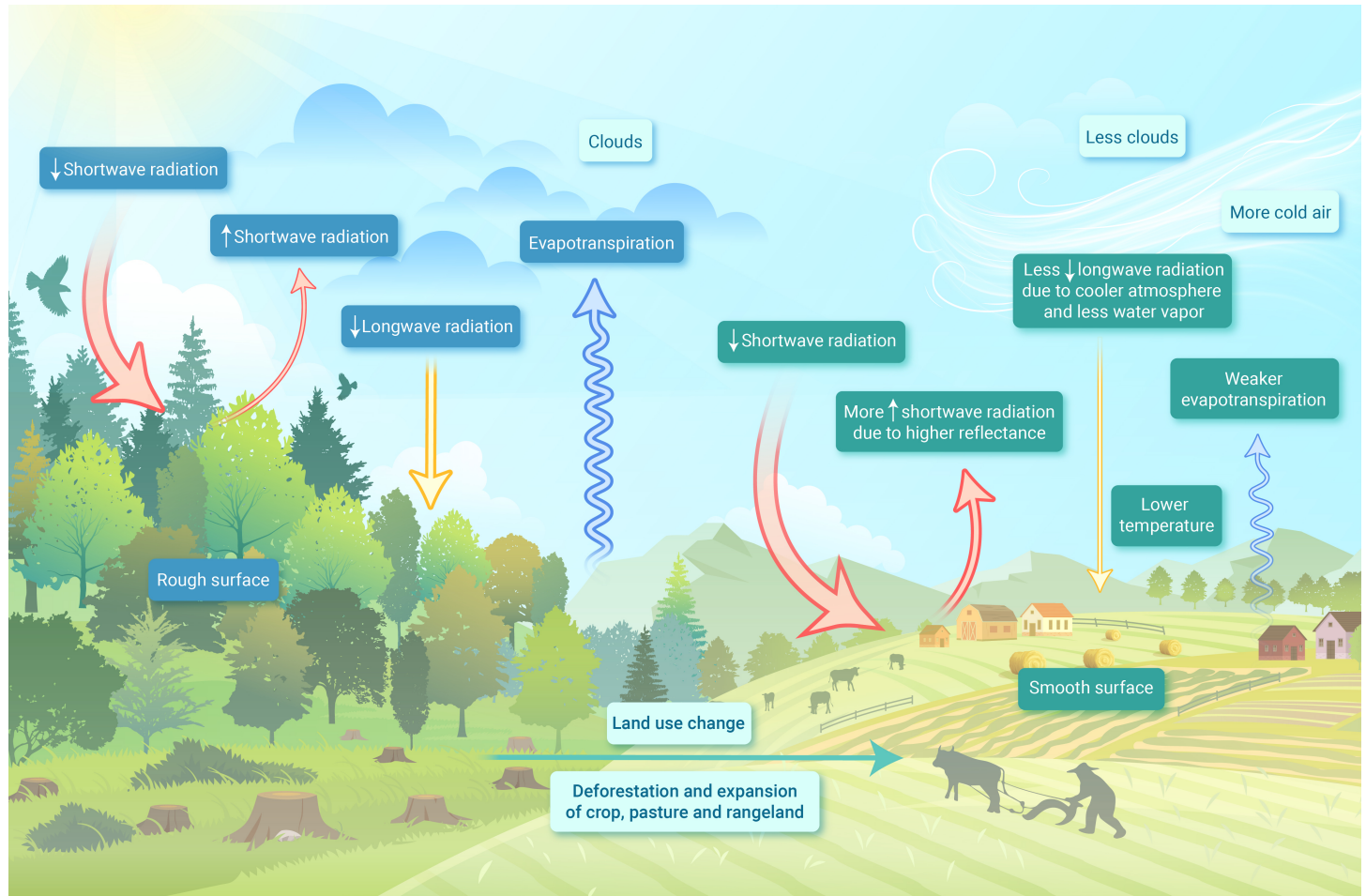
Tao Tang,<sup>1,2,\*</sup> Xuhui Lee,<sup>1</sup> and Keer Zhang<sup>1</sup>

\*Correspondence: [tangtao@mail.iap.ac.cn](mailto:tangtao@mail.iap.ac.cn); [tao.tang@yale.edu](mailto:tao.tang@yale.edu)

Received: March 12, 2024; Accepted: May 27, 2024; Published Online: June 5, 2024; <https://doi.org/10.59717/j.xinn-geo.2024.100079>

© 2024 The Author(s). This is an open access article under the CC BY-NC-ND license (<http://creativecommons.org/licenses/by-nc-nd/4.0/>).

## GRAPHICAL ABSTRACT



## PUBLIC SUMMARY

- We quantified the impact of historical land use and land cover change (LULCC) on extreme temperature.
- LULCC has enhanced cold extremes and alleviated hot extremes over the mid-latitudes of northern hemisphere.
- The strongest changes are observed in the central and eastern North America and Europe.
- These changes are largely the results of climate feedback due to LULCC.



# Historical land use and land cover change reduced the temperature of cold extremes more than that of hot extremes

Tao Tang,<sup>1,2,\*</sup> Xuhui Lee,<sup>1</sup> and Keer Zhang<sup>1</sup>

<sup>1</sup>School of the Environment, Yale University, New Haven CT 06511, USA

<sup>2</sup>Science Center for Earth System Numerical Simulation, Institute of Atmospheric Physics, Chinese Academy of Sciences, Beijing 100029, China

\*Correspondence: [tangtao@mail.iap.ac.cn](mailto:tangtao@mail.iap.ac.cn); [tao.tang@yale.edu](mailto:tao.tang@yale.edu)

Received: March 12, 2024; Accepted: May 27, 2024; Published Online: June 5, 2024; <https://doi.org/10.59717/j.xinn-geo.2024.100079>

© 2024 The Author(s). This is an open access article under the CC BY-NC-ND license (<http://creativecommons.org/licenses/by-nc-nd/4.0/>).

Citation: Tang T., Lee X., and Zhang K. (2024). Historical land use and land cover change reduced the temperature of cold extremes more than that of hot extremes. *The Innovation Geoscience* 2(3): 100079.

The impact of historical land use and land cover change (LULCC) on the mean climate has been extensively studied, but its impact on temperature extremes is not well understood. This study investigates the biophysical effect of LULCC on temperature extremes using two sets of model simulations – one with land use fixed at 1850 level and the other with historical LULCC from 1850 to 2014. We find that the historical LULCC has two asymmetric effects: (i) it decreases the temperature of coldest day ( $-0.56 \pm 0.23$  K; mean  $\pm$  std. error) more than that of the hottest day ( $-0.21 \pm 0.07$  K) at the mid-latitudes of northern hemisphere; and (ii) it has a stronger impact in the mid-latitudes of northern hemisphere relative to the tropical region. These changes result largely from an indirect effect of LULCC via changes in clouds, circulations, and the downward longwave radiation. We stress that the indirect effects from climate feedback of LULCC should be considered when implementing reforestation policy.

## INTRODUCTION

Human and natural systems are vulnerable to extreme weather and climatic events. Over the past several decades, cold extremes have been decreasing and hot extremes have been increasing in frequency and intensity.<sup>1</sup> The 5<sup>th</sup> assessment report of Inter-governmental Panel on Climate Change (IPCC) concludes that human activities have modified the intensity and frequency of daily temperature extremes since the mid-20<sup>th</sup> century.<sup>2</sup> One such activity is the land use and land cover change (LULCC), manifested primarily as the loss of primary and secondary land (psl) and concomitant expansion of cropland, pasture and rangeland, providing food, energy and timber to human society. Specifically, psl decreased by  $\sim 21.3\%$  of the global land (31.7 Mkm<sup>2</sup>) in 2014 relative to 1850, including roughly 7.1 Mkm<sup>2</sup> forest loss. In the same period, cropland, pasture and rangeland expanded extensively, with a fractional change of +6.4% (crop), +3.5% (pastureland) and +10.7% (rangeland; Figure 1).

LULCC influences the climate system biogeochemically by changing atmospheric greenhouse gas concentrations and biophysically by changing surface properties. When forests are replaced with cropland and pastureland, the surface albedo will increase, leading to cooling of the surface. On the other hand, deforestation reduces surface evapotranspiration (ET), which causes warming. The balance of these two competing biophysical effects is latitudinal dependent.<sup>4-6</sup>

There is a large body of literature on the climate impact of LULCC. In observational studies, the climate impact of deforestation is quantified by comparing temperature observed at a forest with that at a nearby open land, assuming the same background climate at both locations.<sup>4,7</sup> By equating the difference from observations made at the same time to changes of land use over time, these studies imply a space-for-time substitution. The space-for-time strategy has two drawbacks. The first is that a 100% deforestation is assumed in such comparison (forest vs. open land), which is usually not the case in reality; The second is that the observational results reveal direct effects of surface changes but miss indirect effects of LULCC. The direct effect is associated with changes of surface albedo, roughness and ET efficiency and arises directly from land cover changes, with the atmospheric conditions unchanged.<sup>8,9</sup> The indirect effect is caused by the feedback from changes in the background climate, such as changes of clouds, circulation, and downward radiation, which is cancelled out in the space-for-time strategy.

Factorial experiment method using fully-coupled simulations with and without LULCC can be used to derive the surface climate changes including both direct and indirect effects of LULCC. In idealized model simulations, deforestation is usually applied uniformly at a high rate (e.g., 50%) to generate a strong signal.<sup>10,11</sup> Such idealized simulations provide mechanistic understanding of the LULCC impact, but they are not a realistic representation of historical LULCC which occurred gradually over time. Besides, the climatic impacts of slow and prolonged deforestation (e.g., 1% decrease annually) are different from those of sudden deforestation.<sup>12-15</sup> Moreover, the temperature response may be greater in the regions where LULCC is more intense as the historical LULCC is highly heterogeneous rather than uniform (Figure 1; Lawrence & Vandecar, 2015<sup>16</sup>). Thus, a realistic assessment of LULCC impacts is still lacking and imperative.

In addition to mean temperature, LULCC also influences temperature extremes. Results of modeling studies, however, depend on whether indirect effects are included. For example, Lejeune et al. (2018)<sup>17</sup> reported an enhancement of hot extremes due to LULCC in the northern mid-latitudes while Chen and Dirmeyer (2019)<sup>18</sup> found the opposite. The former study used a linear regression technique, which includes direct effect only while the latter used coupled model simulation, including both direct and indirect effects. Almost all published modeling studies investigating total effects are based on single model simulations,<sup>18-22</sup> which may be subject to model biases and structural uncertainties.<sup>23</sup>

In this study, we investigate the impact of historical LULCC on daily and monthly temperature extremes with seven climate models. Two sets of fully-coupled simulations -- one with land use held at the 1850 level and the other forced with gradual LULCC over the historical period -- are compared. Results are presented as multi-model mean (MMM) values for both hot extremes and cold extremes and in intensity and frequency. The methodology deployed in this study offers several advantages: (i) inclusion of indirect effects arising from atmospheric feedback rather than just direct effects as in space-for-time studies; (ii) a more realistic assessment of historical LULCC impact than idealized modeling studies; (iii) reduced model bias and easier determination of whether regional changes are greater than structural uncertainties of climate models.<sup>23-25</sup> Our results show that historical LULCC lowers both cold and hot temperature indices over the mid-latitudes of northern hemisphere (mid-NH), with a larger decrease from the former. In addition, we also show how LULCC changes extreme temperatures by modifying the surface energy budget and circulations.

## MATERIALS AND METHODS

### CMIP6 model data

Two simulations per model were employed to quantify the LULCC impact. The first simulation is the standard historical simulation including all anthropogenic (e.g., greenhouse gases, aerosols and LULCC) and natural forcing (e.g., solar and volcanic activities), in which LULCC is prescribed by the Land-Use Harmonization dataset.<sup>3</sup> The second is the hist-noLu simulation from the Land Use Model Intercomparison Project,<sup>26</sup> in which the forcing is identical to the historical experiment, but with land use fixed at the 1850 level. The LULCC data in all CMIP6 models is provided by Hurtt et al.<sup>3</sup> In this product, GLM2 model (the model underlying the dataset) computes subgrid-scale land use states and corresponding transition rates in each gridcell as a function of the land surface at the previous time step and a transition matrix. As a result, each land cover type is assigned with a fraction in each gridcell, which

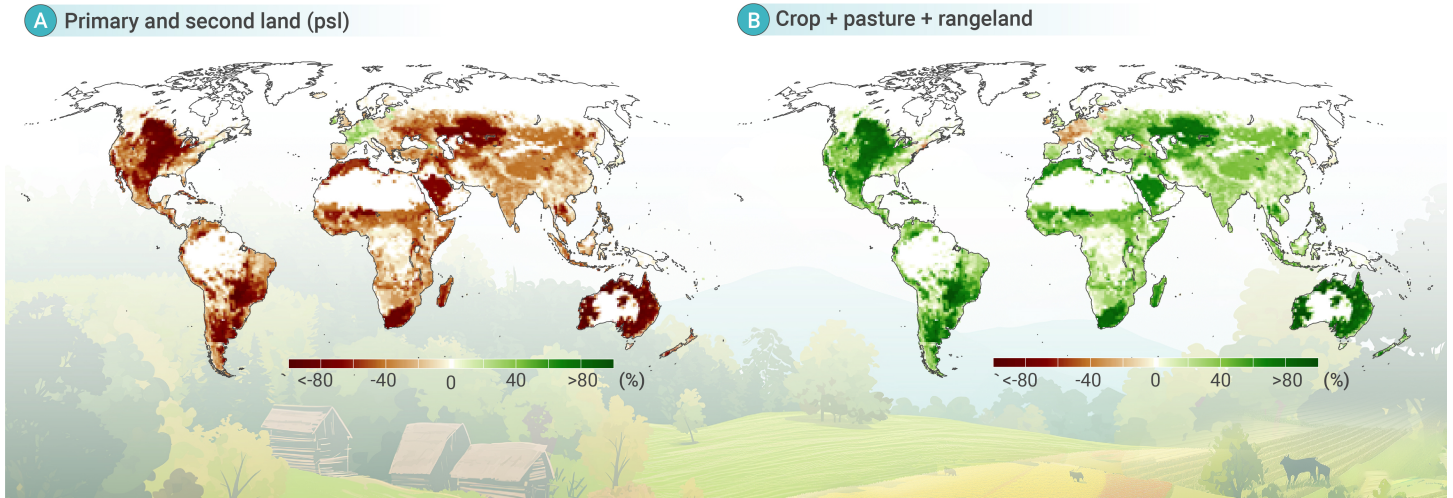


**Figure 1.** Spatial pattern of fractional changes of land type in each gridcell in 1995-2014 relative to 1850 (A) primary and secondary land, (B) combination of cropland, pasture and rangeland. Data is from Hurtt et al.<sup>3</sup>

varies annually. The input land use map is based on the History of the Global Environment database (HYDE 3.2) that provides long-term and spatially explicit time series of population and land use reconstructions from 10000 BC to the present.<sup>27</sup> In HYDE 3.2, observed land use and population data were used where observations available (e.g., satellite products and Food and Agriculture Organization statistics). Before the observation era, per capita land use was estimated and then modelled back in time and also implemented in some countries by subnational statistics, assuming that they were not constant but followed a curved trajectory. Please refer to Klein Goldewijk et al.<sup>27</sup> and Hurtt et al.<sup>3</sup> for detailed information regarding the historical land use map. It is also noted that not all models could fully implement this LULCC data, but with different levels and complexities depending on their own configurations (e.g., some models do not have pasture). These simulations were run in fully-coupled mode from 1850-2014, and the period of 1995-2014 were analyzed in this study. Seven CMIP6 models archived daily 2-m temperature data are employed in this study (Table S1).

## Methods

The temperature of the coldest day ( $T_{cd}$ ), the coldest month ( $T_{cm}$ ), the hottest day ( $T_{hd}$ ) and the hottest month ( $T_{hm}$ ) of each year are extracted for each gridcell. The LULCC impact was quantified as differences in these temperature variables. For example, the impact of LULCC on the coldest day is defined as:

$$\Delta T_{cd} = \overline{T_{cd}(\text{historical})}_{1995-2014} - \overline{T_{cd}(\text{hist} - \text{noLu})}_{1995-2014} \quad (1)$$

In (1),  $\Delta$  is the difference of  $T_{cd}$  due to LULCC impact (historical minus hist-noLu) while the overbars represent the mean value of 1995-2014. The LULCC signal increases gradually with time, reaching maximum in the last several decades. The period of 1995-2014 can clearly demonstrate the signal (Figure S1). All models are linearly regridded to the resolution of  $0.94^\circ$  (latitude)  $\times$   $1.25^\circ$  (longitude) before processing. We first computed these differences for each gridcell in each model and then averaged the results to obtain MMM values, giving equal weight to each model. A boot-strap technique was utilized to determine if the MMM values are different from zero with statistical significance at the gridcell level. The seven model values were sampled seven times randomly with replacement to obtain a mean value. The process was repeated for 500 times to construct a 95% confidence interval. The MMM changes are considered significant if zero falls outside the confidence interval.

To examine the change in the frequency of temperature extremes, we first obtained the temperature value colder than a preset percentile (e.g. colder than 90% of daily temperature) over 1995-2014 in the hist-noLu simulation ( $T_0$ ) and the number of days colder than  $T_0$  in this simulation. We then calculated the number of days colder than  $T_0$  in the historical simulation with LULCC forcing. The difference in the number of days colder than  $T_0$  is

considered to be caused by the LULCC activity. The same process was also repeated for hot days. A similar bootstrap was used to determine whether the changes in extreme frequencies are statistically significant.

The concentrations of greenhouse gases in the hist-noLu experiment are identical to those in the historical experiment. In other words, the historical LULCC does not modify the carbon cycle in this simulation. The temperature difference between the two experiments is caused solely by biophysical changes.

The biophysical changes have direct and indirect effects on the surface air temperature. To separate the direct and indirect effects of LULCC, we employed a multi-linear regression model to estimate the direct effects.<sup>17</sup> Specifically, for each grid cell  $i$ , we selected a  $5 \times 5$  window centered on this grid cell and then regressed the temperature change against four spatial predictors: the fraction change of psl ( $\Delta psl$ ), latitude ( $lat$ ), longitude ( $lon$ ), and elevation ( $elev$ ), obtaining:

$$\Delta T_{cd} = \beta_0 + \beta_1 \times \Delta psl + \beta_2 \times lat + \beta_3 \times lon + \beta_4 \times elev \quad (2)$$

where  $\Delta T_{cd}$  is the total effect obtained from the Equation (1).  $\Delta T_{cd}$ ,  $\Delta psl$ ,  $lat$ ,  $lon$  and  $elev$  are vectors containing up to 25 values centered on grid cell  $i$ , and the  $\beta$  coefficients are specific to the grid cell  $i$ . The direct effect of psl change on  $\Delta T_{cd}$  at the grid cell  $i$  is then estimated by scaling the coefficients with the psl fraction change at the grid cell  $i$ :

$$\Delta T_{cd, \text{direct}}(i) = \beta_1 \times \Delta psl(i) \quad (3)$$

The indirect effect at the grid cell  $i$  is then estimated as:

$$\Delta T_{cd, \text{indirect}}(i) = \Delta T_{cd}(i) - \Delta T_{cd, \text{direct}}(i) \quad (4)$$

In Equation (4),  $\Delta T_{cd}(i)$  is from the Equation (1), representing the total effect at the grid cell  $i$ . We applied this method to all land grid cells with the  $5 \times 5$  window containing at least 13 valid values and repeat this process to all the temperature indices. The inclusion of the other three predictors on top of the psl change aims to minimize the signals from natural climatic gradients within the  $5 \times 5$  box. This method assumes that the indirect effects from the large-scale circulation changes have a similar impact on the  $5 \times 5$  box.<sup>17,28</sup> It is also acknowledged that some small-scale indirect effects within this  $5 \times 5$  box cannot be fully excluded. Therefore, the direct effects calculated with this approach may be slightly overestimated.

A surface energy budget analysis is also employed in this study. The incoming radiation at the surface ( $R_{in}$ ) is calculated as:

$$R_{in} = \text{netSW} + \downarrow \text{LW} \quad (5)$$

In Equation (5), netSW is the net shortwave (SW) radiation at the surface and  $\downarrow \text{LW}$  is the downward longwave (LW) radiation at the surface. Both SW and LW radiation can be separated into cloud radiative effects and clear-sky

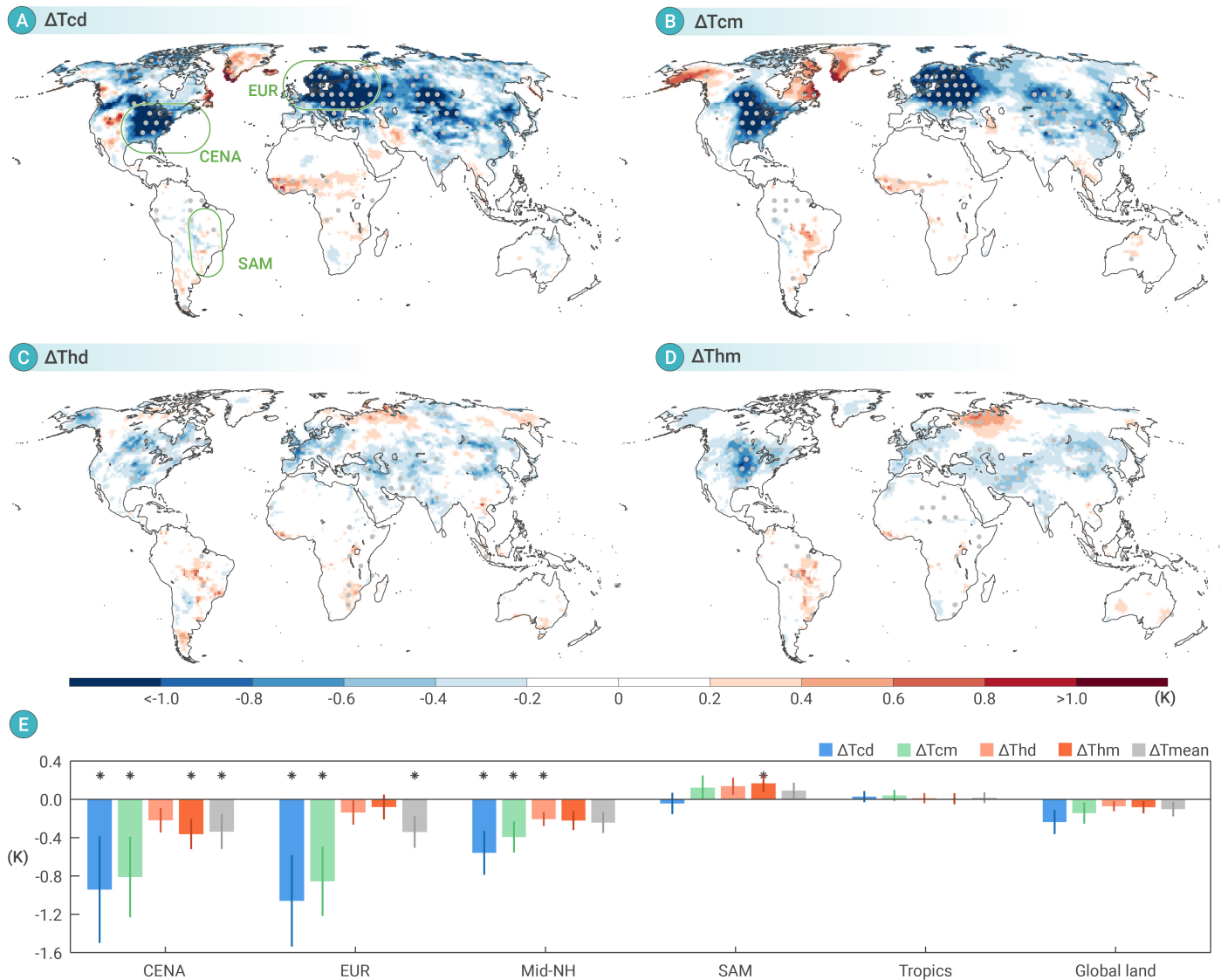


**Figure 2. Spatial pattern of MMM changes of extreme temperature indices** (A) changes of the coldest day ( $\Delta T_{cd}$ ), (B) changes of the coldest month ( $\Delta T_{cm}$ ), (C) changes of the hottest day ( $\Delta T_{hd}$ ) and (D) changes of the hottest month ( $\Delta T_{hm}$ ). (E) shows the MMM domain-averaged changes of extreme temperatures and mean temperature ( $T_{mean}$ ) for the central and eastern North America (CENA), Europe (EUR), mid-latitudes of Northern Hemisphere (mid-NH), South America (SAM), Tropics and whole global land (without Antarctica). Green boxes in (A) define the regions of CENA, EUR, and SAM, respectively. The gray dots in (A)-(D) denote significant changes at  $p = 0.05$  level. Dots are shown every 5 columns and rows for clarity. The error bars in (E) represent one standard error of MMM and \* in (E) denotes the corresponding domain-averaged changes are significant at  $p = 0.05$  level.

conditions.<sup>29</sup>  $R_{in}$  can be rearranged as:

$$R_{in} = \text{netSW}_{\text{clearsky}} + \downarrow \text{LW}_{\text{clearsky}} + \text{CRE} \quad (6)$$

In Equation (6),  $\text{netSW}_{\text{clearsky}}$  is the net SW radiation under clear-sky conditions,  $\downarrow \text{LW}_{\text{clearsky}}$  is  $\downarrow \text{LW}$  radiation under clear-sky conditions, and CRE is the cloud radiative effects.  $R_{in}$  is balanced by outgoing LW radiation, sensible heat flux (H), latent heat flux (LE) and ground heat flux.

## RESULTS

Figure 2 shows the spatial patterns of the four temperature change variables, along with the domain-averaged changes for the selected regions, over the period of 1995 to 2014. The historical LULCC activity lowers both cold and hot temperature extremes in the Northern Hemisphere (NH) with a larger decrease for cold extremes, especially in the central and eastern North America (CENA, 105°W–51°W, 25°N–49°N) and the Europe (EUR, 9°W–59°E, 46°N–72°N). The domain-averaged  $T_{cd}$  is reduced significantly by  $0.56 \pm 0.23$  K (MMM  $\pm$  s.e.) in the NH mid-latitudes (mid-NH, 30°N–60°N). In the CENA and EUR, the  $T_{cd}$  decreases are  $0.94 \pm 0.56$  K and  $1.06 \pm 0.48$  K, respectively, both of which are statistically significant. Averaged over global land grids (without

Antarctica), the  $T_{cd}$  is reduced by  $0.24 \pm 0.12$  K. In South America (SAM, 60°W–42°W, 2°S–35°S), a region with intense LULCC (Figure 1) and the whole tropical regions (20°S–20°N), however,  $\Delta T_{cd}$  is almost zero, at  $-0.04 \pm 0.06$  K and  $0.03 \pm 0.06$  K, respectively. The coldest month ( $T_{cm}$ ) shows comparable changes as the  $T_{cd}$  (Figures 2B & E), with reductions of  $0.39 \pm 0.16$  K in the mid-NH,  $0.81 \pm 0.42$  K in the CENA and  $0.86 \pm 0.36$  K in the EUR, and insignificant increases of  $0.12 \pm 0.13$  K in the SAM and  $0.04 \pm 0.06$  K in the tropics. The global land mean  $\Delta T_{cm}$  is  $-0.14 \pm 0.11$  K but is not significant. The changes in these cold extremes are larger than the mean temperature changes, most notably in the CENA and the EUR.

In terms of hot extremes, both the  $T_{hd}$  and the  $T_{hm}$  show the same sign of change as the cold extremes in the boreal region, but with much reduced magnitudes (Figures 2C-E), mostly within  $-0.1$  to  $-0.3$  K and statistically insignificant over most of the NH. Statistically significant changes are observed in the CENA for the  $T_{hm}$  ( $-0.36 \pm 0.16$  K) and the mid-NH for the  $T_{hd}$  ( $-0.21 \pm 0.07$  K). In the SAM, the  $T_{hd}$  and the  $T_{hm}$  are increased by  $0.14 \pm 0.09$  K and  $0.17 \pm 0.09$  K, respectively, with the latter being statistically significant. The changes of hot extremes are negligible in the whole tropics. Larger decreases in cold extremes than hot extremes also imply a faster

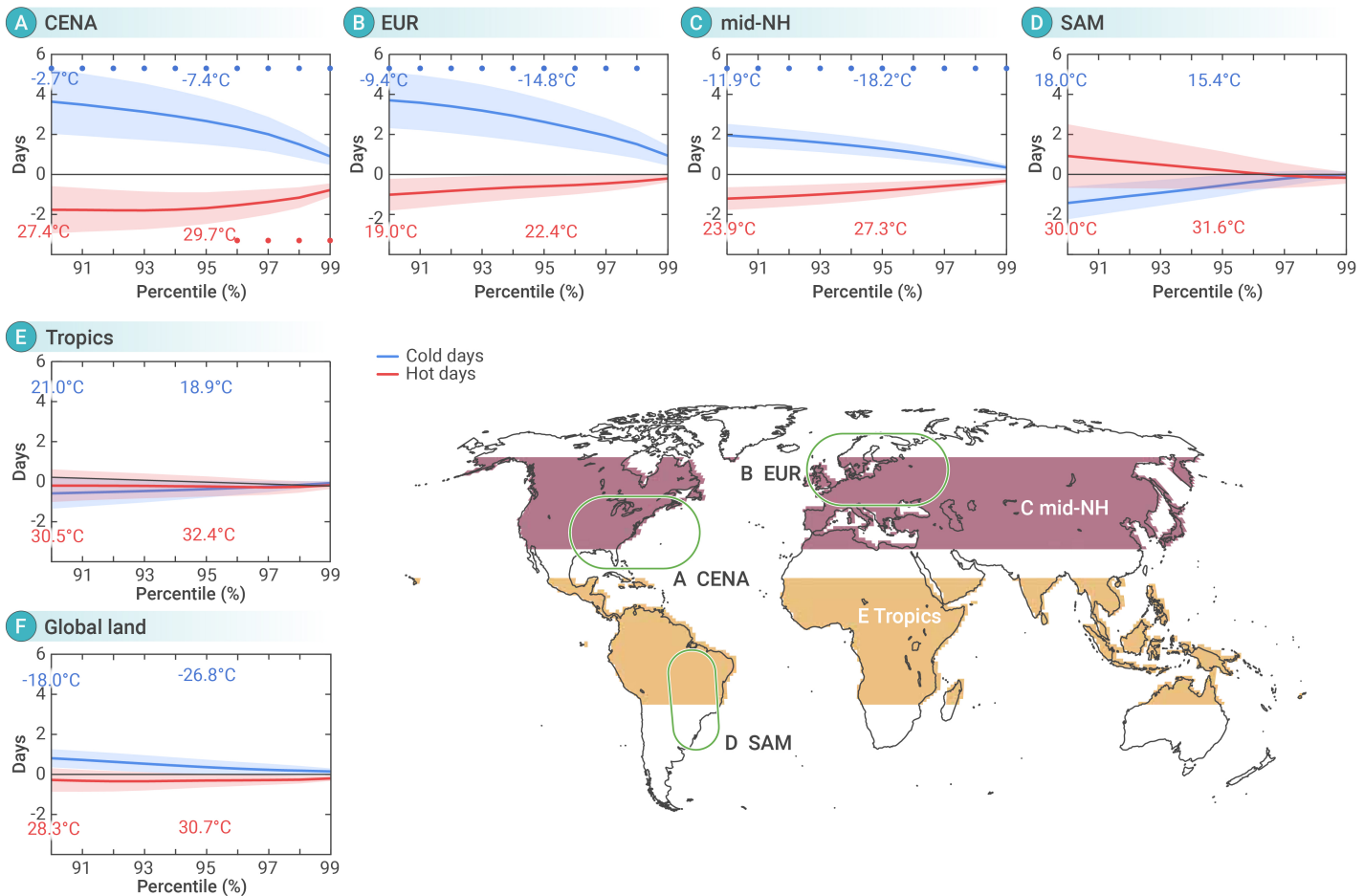


**Figure 3.** Changes in the number of extreme cold (blue) and hot days (red) as functions of percentile for the selected regions (A) central and eastern North America (CENA), (B) Europe (EUR), (C) mid-latitudes of Northern Hemisphere (mid-NH), (D) South America (SAM), (E) Tropics, and (F) whole global land (without Antarctica). Thick solid lines are MMM values and shaded patches are standard error. Dots in the upper and lower x-axis indicate that changes for this percentile are significant at  $p = 0.05$ . The 90% and 95% percentile temperatures in hist-noLu simulation are shown for reference. The world map shows the boundaries of the selected regions.

decreasing rate of cold extremes. The decreasing rates of cold extremes are two to four times higher than hot extremes over the CENA, the EUR and the mid-NH (Figure S1).

The above results reveal that the impact of historical LULCC is asymmetric. The changes are stronger and faster for the cold extremes than for the hot extremes. This asymmetry is also evident in the frequency of extreme temperatures. Figure 3 shows the change in the number of cold and hot extreme days due to historical LULCC activity.

In the CENA, the 90%, 95% and 99% cold temperature is  $-2.7$ ,  $-7.4$  and  $-16.8$  °C in the hist-noLu simulation (Figure 3A). Putting it differently, there are 36.5, 18.3 and 3.7 days per year with daily temperature lower than these values. The number of the coldest 90% days is increased by 3.6 days in the historical experiment than in the hist-noLu simulation (Figure 3A, blue), giving a total of  $36.5 + 3.6$  days with temperature colder than  $-2.7$  °C. The increase in the number of 95% coldest days is 2.7 days, giving a total of  $18.3 + 2.7$  days with daily temperature lower than  $-7.4$  °C. The number of 99% coldest days is increased by roughly 1.0 day per year, giving a total of  $3.7 + 1.0$  days. All these changes are statistically significant at  $p = 0.05$  level. The EUR shows similar increasing frequency of cold extremes as the CENA (Figure 3B). In the mid-NH, the increase in the number of the 90% and the 95% coldest days is halved, at about 2 days and 1.3 days per year, respectively (Figure 3C). Globally, the change in the frequency of cold days is quite limited: the number of the 90% coldest days is increased by 0.8 days, and the change is not statistically significant (Figure 3F). The changes in cold day frequency are insignificant in the tropics and the SAM.

The change in the frequency of hot days is smaller than that of the cold days. In the CENA, the number of the 90% hottest days is decreased by

approximately 1.8 days. Here the 90% hottest days are days with daily temperature greater than  $27.4$  °C. In this region, LULCC decreases the number of days with daily temperature greater than  $27.4$  °C from 36.5 days to 34.7 days per year. The numbers of the 95% to 99% hottest days are decreased statistically significant by roughly 1 day per year (Figure 3A, red). The number of the 90% hottest days is also decreased by roughly 1 day in both the EUR and the mid-NH (Figure 3B-C). In contrast, the frequency of 90% hottest days is increased by roughly 1 day per year in the SAM, but the change is not statistically significant. The frequency changes of hottest days are mostly negligible in the tropical regions and the whole global land.

Figure 4 shows the direct and indirect effects of LULCC on the four extreme temperature indices (see Methods). In the CENA, the direct effects of LULCC are mostly cooling due to albedo effect in all four indices and this cooling effect is further reinforced by the indirect effects, with the latter being two to four times larger than the former. In the EUR, the direct effects are negligible, indicating that the total effect is dominated by the indirect effects. This is also the case for the whole mid-NH. In the SAM, however, the warming induced by direct effects are either counteracted or enhanced by indirect effects, and the total effects are shaped by both direct and indirect effects, with varying contributions in different indices.

During the boreal winter (DJF), the change of all incoming energy terms and  $\Delta LE$  are highly correlated with  $\Delta T_{cm}$  in the CENA (Figure 5A). The cooling over the CENA is mainly caused by albedo effect and then further reinforced by reduced  $\downarrow LW_{clearsky}$  due to cooler atmosphere, despite some offset by  $\Delta CRE$  and  $\Delta LE$  (Figures 5 & S2). In the EUR,  $\Delta \downarrow LW_{clearsky}$  has the highest correlation coefficient with  $\Delta T_{cm}$  ( $r = 0.79$ ), highlighting the crucial role of indirect effects. Previous studies reported a strong control of circulation

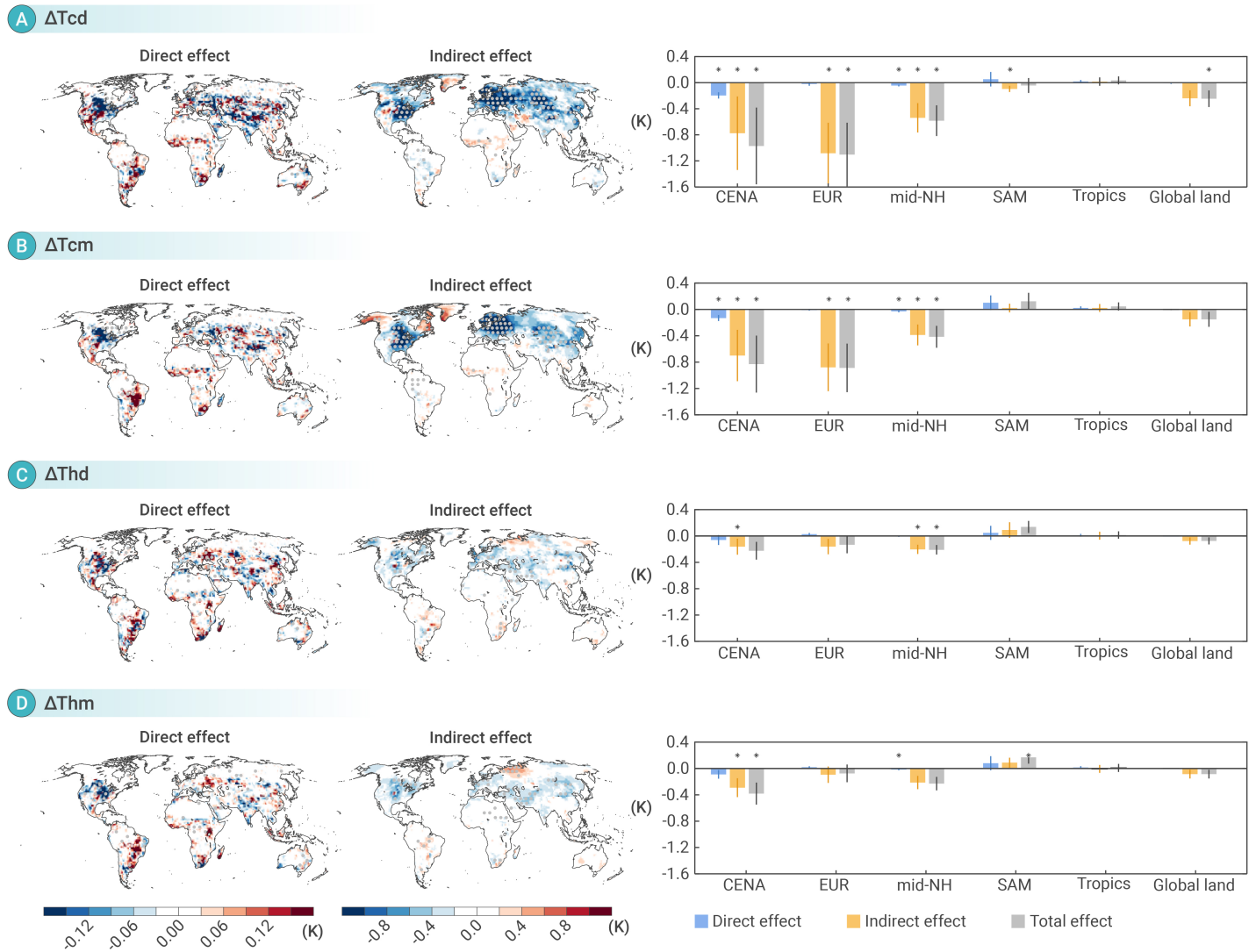


**Figure 4.** Direct (left column) and indirect (middle column) effects of LULCC on the four temperature indices (A) changes of the coldest day ( $\Delta T_{cd}$ ), (B) changes of the coldest month ( $\Delta T_{cm}$ ), (C) changes of the hottest day ( $\Delta T_{hd}$ ) and (D) changes of the hottest month ( $\Delta T_{hm}$ ). The right column is domain-averaged values for the selected regions. The gray dots in the left and middle columns denote significant changes at the  $p = 0.05$  level, which are shown every 5 columns and rows for clarity. The error bars in the right column represent standard error and the \* denotes significant changes of domain-averaged values at the  $p = 0.05$  level. Note the different color scales between the left and the middle column.

patterns on the extreme temperature over these regions.<sup>31–33</sup> Our analyses suggest a negative Arctic Oscillation-like circulation pattern over North Atlantic due to LULCC, in which more cold air from high latitudes penetrates into the EUR and the CENA, thereby contributing to enhanced cold extremes (Figure 5C). It is worth noting that circulations and  $\downarrow LW_{clearsky}$  are not exclusive, as more cold air advection can decrease  $\downarrow LW_{clearsky}$ . The results are similar to the CENA and the EUR when averaged over the whole mid-latitudes (Figure 5A). During the boreal summer (JJA), the cooling in the CENA is mainly contributed by enhanced LE and further amplified by  $\Delta \downarrow LW_{clearsky}$  and  $\Delta CRE$ . In the EUR, the indirect effects dominate again, with  $\Delta \downarrow LW_{clearsky}$  and  $\Delta CRE$  have the highest correlation coefficients (Figure 5B). The circulation changes, however, are much smaller compared with winter months. In the lower latitudes, there is no obvious seasonality. It is therefore more appropriate to examine the energy changes on annual scale. In the SAM, reduced LE caused initial warming in  $\Delta T_{hm}$  (Figure 4D), and this warming effect is further modified by  $\Delta \downarrow LW_{clearsky}$  and  $\Delta CRE$  (Figure S2), with  $\Delta \downarrow LW_{clearsky}$  and  $\Delta LE$  have the highest correlation coefficients (Figure 5B).

Our analyses show that the magnitudes of direct effects of LULCC are similar in the mid-NH and the tropics (Figure 4) and the varying latitudinal pattern of extreme temperature response is mainly shaped by indirect effects, with the strongest control from  $\Delta \downarrow LW_{clearsky}$  and to a lesser extent, from clouds ( $\Delta CRE$ ). The latitudinal pattern is further evidenced by the higher  $r$

values in the mid-NH regions compared with lower  $r$  values in the tropical regions (Figure 5). On top of the latitudinal pattern, the asymmetrical response of cold and hot extremes is also due to the different indirect effects, as indirect effects are 2–4 times larger in cold extremes than in hot extremes (Figure 4). The crucial role of indirect effects stress that the climate feedback of LULCC should be considered when planning reforestation policy.<sup>34–35</sup>

## CONCLUSIONS AND DISCUSSIONS

By using coupled model simulations with historical LULCC, our study confirms that historical LULCC cools the land surface biophysically. Specifically, LULCC decreases the temperature of the coldest day by  $0.56 \pm 0.23$  K and that of the coldest month by  $0.39 \pm 0.16$  K at the mid-latitudes of northern hemisphere. At these latitudes, the number of the 90% coldest day is increased by 2 days and the number of the 95% coldest day increased by roughly 1 day annually. The strongest cooling is seen in the central and eastern North America and the Europe, two regions with intense historical LULCC. These two regions experience a temperature reduction of over 0.8 K in both the  $T_{cd}$  and the  $T_{cm}$ , and an increase of 4 days in the number of the 90% coldest day annually. The hot extremes also show decreasing trends, but the trends are much weaker. The  $T_{hm}$  decreased by  $0.36 \pm 0.16$  K in the central and eastern North America and the  $T_{hd}$  is decreased by  $0.21 \pm 0.07$  K over the whole mid-latitudes of the northern hemisphere. The Amazon (SAM)

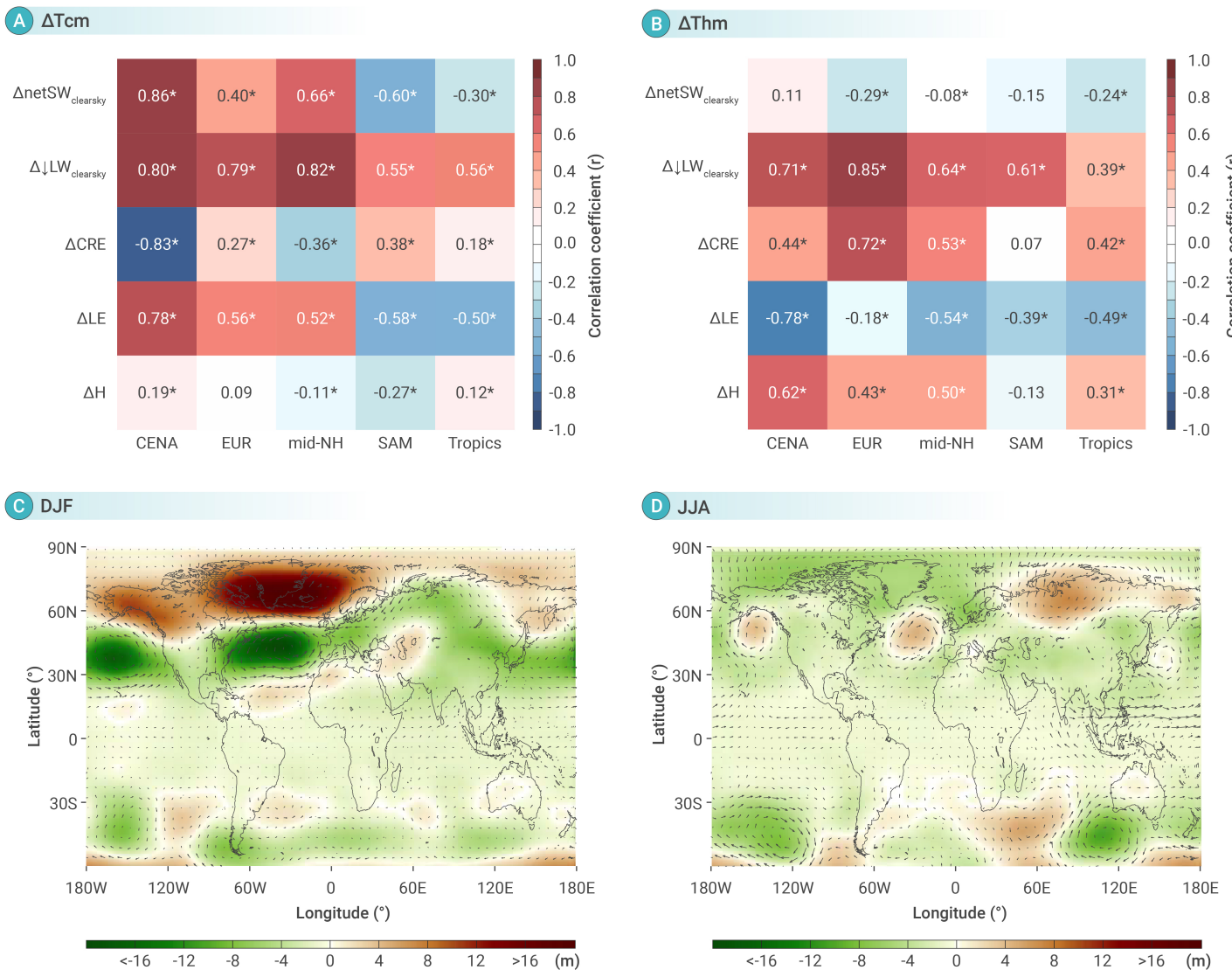


**Figure 5. Changes of surface energy budget and circulations** (A) Correlation coefficients ( $r$ ) between  $\Delta T_{cm}$  and each energy component in DJF for each region. (B) Same as (A), but for  $\Delta T_{hm}$  in JJA. For the SAM and the tropics, the annual mean values are used in both panels. \* indicates  $p < 0.001$ . (C) Changes of geopotential height at 500 hPa (color shaded) and winds at 850 hPa (vectors) in DJF. (D) Same as (C), but for JJA.

experienced slight exacerbation in the hottest month whereas the whole tropical regions show negligible changes for both cold and hot extremes. These changes are dictated by the indirect effects from climate feedback, mainly the changes of radiation due to  $\downarrow \text{LW}_{\text{clearsky}}$ , CRE and circulations.

We repeated our analyses to the boreal spring and fall seasons. The results are similar to Figure 2, but with reduced magnitudes (Figures S3&S4), indicating that the impact of LULCC on extreme temperature is all year round. We also extended the length of study period to 1975–2014, and the results are also similar (Figure S5), implying that our results are robust and not sensitive to the chosen period.

Accompanied agricultural expansion is the diversion of river water and groundwater for irrigation. Irrigation is known to reduce hot extremes by enhancing surface evaporation.<sup>28,36</sup> Among the seven models used in this study, only CESM2 model activated irrigation scheme. The asymmetrical impact of LULCC on cold and hot extremes would be smaller than reported above if all the models allow cropland irrigation (and hence more evaporation in the summer).

The signal strengths reported here are different from those reported by Li et al.<sup>4</sup> and Alkama and Cescaati.<sup>37</sup> The main reason is that our results include both direct and indirect effects of LULCC, while those two studies consider only direct effects. When examining the direct effects only, our pattern is

partially similar to these studies (Figure 4, left column). The slight differences between our result and these two observation-based studies may be caused by (i) different temperature indices investigated; (ii) different sampling frequency of data (monthly mean vs. 8-day or 16-day interval); (iii) different sky conditions (all-sky vs. clear-sky); (iv) different study period; (v) different temperature (2m air temperature vs. radiometric temperature); and (vi) different LULCC (psl loss in this study and forest vs. open land in previous study).

The uncertainty of a modeling study comes from three sources: (i) internal variability (natural variability from the climate system, such as El Niño); (ii) structural uncertainty (different choices in parameterization and representation of unsolved processes); and (iii) different forcing scenarios.<sup>38</sup> In this study, the main uncertainties are associated with internal variability and structural uncertainty. Both uncertainties were sampled in the multi-model ensemble approach,<sup>23</sup> which is reported to be better than single model simulations.<sup>25</sup> For example, the MIROC model shows a 0.83 K increase in the Tcd in the CENA region. This value is far from the MMM result ( $-0.56 \pm 0.23$  K; Figure 2) and opposite conclusions would be drawn if this model was used alone. This analysis further highlights the importance of the multi-model ensemble approach and lends confidence in our conclusions. However, we acknowledge that the sample size is still limited (seven in total) and some models have shared components (e.g. the CMCC model also employed CLM

as the land surface model as in CESM2), which cannot be treated as independent, implying a reduction in the effective number of sample size.<sup>39</sup> We propose that more model simulations are required in future studies of this kind.

## REFERENCES

- Donat, M.G., Alexander, L.V., Yang, H., et al. (2013). Global land-based datasets for monitoring climatic extremes. *Bull. Am. Meteorol. Soc.* **94**: 997–1006. DOI: 10.1175/BAMS-D-12-00109.1.
- Hartmann, D., Klein Tank, A., Rusticucci, M., et al. (2013). Observations: Atmosphere and surface. Stoker, T. F., Qin, D., Plattner, G.-K. et al., (eds). *Climate change 2013: The physical science basis. Contribution of working group I to the fifth assessment report of the intergovernmental panel on climate change* (Cambridge University Press), pp. 159–254.
- Hurtt, G.C., Chini, L., Sahajpal, R., et al. (2020). Harmonization of global land use change and management for the period 850–2100 (LUH2) for CMIP6. *Geosci. Model Dev.* **13**: 5425–5464. DOI: 10.5194/gmd-13-5425-2020.
- Li, Y., Zhao, M., Motesharrei, S., et al. (2015). Local cooling and warming effects of forests based on satellite observations. *Nat. Commun.* **6**: 6603. DOI: 10.1038/ncomms7603.
- Perugini, L., Caporaso, L., Marconi, S., et al. (2017). Biophysical effects on temperature and precipitation due to land cover change. *Environ. Res. Lett.* **12**: 053002. DOI: 10.1088/1748-9326/aa6b3f.
- Tang, T., Lee, X., Zhang, K., et al. (2023). Biophysical impact of land-use and land-cover change on subgrid temperature in CMIP6 models. *J. Hydrometeorol.* **24**: 373–388. DOI: 10.1175/JHM-D-22-0073.1.
- Lee, X., Goulden, M.L., Hollinger, D.Y., et al. (2011). Observed increase in local cooling effect of deforestation at higher latitudes. *Nature* **479**: 384–387. DOI: 10.1038/nature10588.
- Davin, E.L. and de Noblet-Ducoudré, N. (2010). Climatic impact of global-scale deforestation: Radiative versus nonradiative processes. *J. Climate* **23**: 97–112. DOI: 10.1175/2009JCLI3102.1.
- Chen, L. and Dirmeyer, P.A. (2016). Adapting observationally based metrics of biogeophysical feedbacks from land cover/land use change to climate modeling. *Environ. Res. Lett.* **11**: 034002. DOI: 10.1088/1748-9326/11/3/034002.
- Davin, E.L., Rechid, D., Breil, M., et al. (2020). Biogeophysical impacts of forestation in Europe: first results from the LUCAS (Land Use and Climate Across Scales) regional climate model intercomparison. *Earth Syst. Dynam.* **11**: 183–200. DOI: 10.5194/esd-11-183-2020.
- Boysen, L.R., Brovkin, V., Pongratz, J., et al. (2020). Global climate response to idealized deforestation in CMIP6 models. *Biogeosciences* **17**: 5615–5638. DOI: 10.5194/bg-17-5615-2020.
- Findell, K.L., Knutson, T.R., and Milly, P.C.D. (2006). Weak simulated extratropical responses to complete tropical deforestation. *J. Climate* **19**: 2835–2850. DOI: 10.1175/JCLI3737.1.
- Avissar, R. and Werth, D. (2005). Global hydroclimatological teleconnections resulting from tropical deforestation. *J. Hydrometeorol.* **6**: 134–145. DOI: 10.1175/JHM406.1.
- Bala, G., Caldeira, K., Wickett, M., et al. (2007). Combined climate and carbon-cycle effects of large-scale deforestation. *Proc. Natl. Acad. Sci. USA* **104**: 6550–6555. DOI: 10.1073/pnas.0608998104.
- Zhang, H., Henderson-Sellers, A., and McGuffie, K. (2001). The compounding effects of tropical deforestation and greenhouse warming on climate. *Climatic Change* **49**: 309–338. DOI: 10.1023/A:1010662425950.
- Lawrence, D. and Vandecar, K. (2015). Effects of tropical deforestation on climate and agriculture. *Nat. Clim. Change* **5**: 27–36. DOI: 10.1038/nclimate2430.
- Lejeune, Q., Davin, E.L., Gudmundsson, L., et al. (2018). Historical deforestation locally increased the intensity of hot days in northern mid-latitudes. *Nat. Clim. Change* **8**: 386–390. DOI: 10.1038/s41558-018-0131-z.
- Chen, L. and Dirmeyer, P.A. (2019). The relative importance among anthropogenic forcings of land use/land cover change in affecting temperature extremes. *Clim. Dynam.* **52**: 2269–2285. DOI: 10.1007/s00382-018-4250-z.
- Christidis, N., Stott, P.A., Hegerl, G.C., et al. (2013). The role of land use change in the recent warming of daily extreme temperatures. *Geophys. Res. Lett.* **40**: 589–594. DOI: 10.1002/grl.50159.
- Findell, K.L., Berg, A., Gentile, P., et al. (2017). The impact of anthropogenic land use and land cover change on regional climate extremes. *Nat. Commun.* **8**: 989. DOI: 10.1038/s41467-017-01038-w.
- Betts, R.A. (2001). Biogeophysical impacts of land use on present-day climate: Near-surface temperature change and radiative forcing. *Atmos. Sci. Lett.* **2**: 39–51. DOI: 10.1006/asle.2001.0023.
- Davin, E.L., de Noblet-Ducoudré, N., and Friedlingstein, P. (2007). Impact of land cover change on surface climate: Relevance of the radiative forcing concept. *Geophys. Res. Lett.* **34**: L13702. DOI: 10.1029/2007GL029678.
- Flato, G., Marotzke, J., Abiodun, B., et al. (2013). Evaluation of climate models. T.F. Stoker, D. Qin, G.-K. Plattner, et al., eds. *Climate change 2013: The physical science basis. Contribution of working group I to the fifth assessment report of the intergovernmental panel on climate change* (Cambridge University Press), pp. 741–866.
- Yun, W.T., Stefanova, L., and Krishnamurti, T.N. (2003). Improvement of the multimodel superensemble technique for seasonal forecasts. *J. Climate* **16**: 3834–3840. DOI: 10.1175/1520-0442(2003)016<3834:IOTMST>2.0.CO;2.
- Sillmann, J., Kharin, V.V., Zhang, X., et al. (2013). Climate extremes indices in the CMIP5 multimodel ensemble: Part 1. *J. Geophys. Res. Atmos.* **118**: 1716–1733. DOI: 10.1002/jgrd.50203.
- Lawrence, D.M., Hurtt, G.C., Arneth, A., et al. (2016). The land use model intercomparison project (LUMIP) contribution to CMIP6: Rationale and experimental design. *Geosci. Model Dev.* **9**: 2973–2998. DOI: 10.5194/gmd-9-2973-2016.
- Klein Goldewijk, K., Beusen, A., Doelman, J., et al. (2017). Anthropogenic land use estimates for the Holocene – HYDE 3.2. *Earth Syst. Sci. Data* **9**: 927–953. DOI: 10.5194/essd-9-927-2017.
- Thiery, W., Visser, A.J., Fischer, E.M., et al. (2020). Warming of hot extremes alleviated by expanding irrigation. *Nat. Commun.* **11**: 290. DOI: 10.1038/s41467-019-14075-4.
- Ramanathan, V., Cess, R.D., Harrison, E.F., et al. (1989). Cloud-radiative forcing and climate: results from the Earth radiation budget experiment. *Science* **243**: 57–63. DOI: 10.1126/science.243.4887.57.
- Clark, J.P., Clothiaux, E.E., Feldstein, S.B., et al. (2021). Drivers of global clear sky surface downwelling longwave irradiance trends from 1984 to 2017. *Geophys. Res. Lett.* **48**: e2021GL093961. DOI: 10.1029/2021GL093961.
- Chen, S., Wu, R., Chen, W., et al. (2020). Coherent interannual variations of springtime surface temperature and temperature extremes between Central-Northern Europe and Northeast Asia. *J. Geophys. Res. Atmos.* **125**: e2019JD032226. DOI: 10.1029/2019JD032226.
- Chen, S., Wu, R., Song, L., et al. (2018). Combined influence of the arctic oscillation and the scandinavia pattern on spring surface air temperature variations over Eurasia. *J. Geophys. Res. Atmos.* **123**: 9410–9429. DOI: 10.1029/2018JD028685.
- Horton, D.E., Johnson, N.C., Singh, D., et al. (2015). Contribution of changes in atmospheric circulation patterns to extreme temperature trends. *Nature* **522**: 465–469. DOI: 10.1038/nature14550.
- Zhu, Y., Wang, D., Smith, P., et al. (2022). What can the Glasgow Declaration on Forests bring to global emission reduction. *The Innovation* **3**: 100307. DOI: 10.1016/j.xinn.2022.100307.
- Liang, S., Liang, L., Wang, D., et al. (2024). Dryland forestation: Uncovering the carbon sequestration potential. *The Innovation Geoscience* **2**: 100058. DOI: 10.59717/j.xinn-geo.2024.100058.
- Cook, B.I., Puma, M.J., and Krakauer, N.Y. (2011). Irrigation induced surface cooling in the context of modern and increased greenhouse gas forcing. *Clim. Dynam.* **37**: 1587–1600. DOI: 10.1007/s00382-010-0932-x.
- Alkama, R. and Cescatti, A. (2016). Biophysical climate impacts of recent changes in global forest cover. *Science* **351**: 600. DOI: 10.1126/science.aac8083.
- Monier, E., Gao, X., Scott, J.R., et al. (2015). A framework for modeling uncertainty in regional climate change. *Climatic Change* **131**: 51–66. DOI: 10.1007/s10584-014-1112-5.
- Tebaldi, C. and Knutti, R. (2007). The use of the multi-model ensemble in probabilistic climate projections. *Philos. Tr. Soc. A* **365**: 2053–2075. DOI: 10.1098/rsta.2007.2076.

## ACKNOWLEDGMENTS

We would like to thank the three anonymous reviewers for their constructive comments. We acknowledge the support from the US National Science Foundation (AGS1933630) and the Chinese Academy of Sciences (E366363601).

## AUTHOR CONTRIBUTIONS

T.T and X.-H.L designed the study. T.T collected the data, performed data analyses and wrote the initial manuscript. All authors contributed to the results interpretation and manuscript polishing.

## DECLARATION OF INTERESTS

The authors declare no competing interests.

## DATA AND CODE AVAILABILITY

All CMIP6 data in this study are freely available from the Earth System Grid Federation (ESGF) portal at <https://esgf-node.lln.gov/projects/cmip6/>. The models used in this study include: ACCESS-ESM1-5 (r1i1p1f1), BCC-CSM2-MR (r1i1p1f1), CESM2 (r1i1p1f1), CMCC-ESM2 (r1i1p1f1), GFDL-ESM4 (r1i1p1f1), MIROC-ES2L (r1i1p1f2) and UKESM1-0-LL (r1i1p1f2). The details of model information could be found in Table S1. LULCC data is obtained from <https://luh.umd.edu/>. The Matlab code for processing the data is available upon reasonable request.

## SUPPLEMENTAL INFORMATION

It can be found online at <https://doi.org/10.59717/j.xinn-geo.2024.100079>